JOURNAL OF PROPULSION AND POWER
Vol. 16, No. 2, March–April 2000

Combustion of Kerosene in Counterflow Diffusion Flames

P. M. Patterson,* A. G. Kyne,† M. Pourkashanian,‡ and A. Williams§
University of Leeds, Leeds, England LS2 9JT, United Kingdom
and
C. W. Wilson¶
Defence Evaluation and Research Agency, Pyestock, Farnborough, Hampshire, England GU14 0LS, United Kingdom

Numerical modeling has become an essential tool in combustion research as a means of predicting combustion performance and pollutant formation, e.g., NO_x and soot. In many combustion models the combustion of a commercial fuel such as kerosene has been represented by single-step empirical expressions. To predict kinetically controlled phenomena, a more detailed chemical kinetic reaction mechanism is required. This paper reports the development of such a mechanism for kerosene, where, for the purposes of modeling, kerosene is assumed to be 89% *n*-decane and 11% toluene. The mechanism is initially validated against experimental jet stirred reactor and rich premixed flame studies to yield satisfactory results. The chemical structure of counterflow diffusion flames is computed using the same mechanism. The effect on the flame structure of increasing both the pressure and the strain rate is explored. The inclusion of a model for thermal radiation using the optically thin approximation demonstrates the large radiative heat losses encountered as the pressure is increased. The calculations form the foundation of a flamelet library for the modeling of turbulent nonpremixed combustion of kerosene under practical conditions.

Nomenclature

a	=	strain rate, s^{-1}
P	=	pressure, atm
Q	=	radiative heat loss term, W m^{-2}
r	=	radial distance, cm
T	=	local flame temperature, K
T_b	=	background or ambient temperature, K
u_∞	=	transverse velocity at oxidizer inlet, cm s^{-1}
v_∞	=	tangential velocity at oxidizer inlet, cm s^{-1}
x	=	axial distance, cm
κ	=	gas mixture absorption coefficient, m^{-1}
ξ	=	mixture fraction
ξ_S	=	stoichiometric mixture fraction
ρ_{fuel}	=	density of fuel, g cm^{-3}
ρ_{oxid}	=	density of oxidizer, g cm^{-3}
σ	=	Stefan–Boltzmann constant, 5.669×10^{-8} W m^{-2} K^{-4}
τ	=	mean residence time, s
ϕ	=	equivalence ratio

Introduction

THE formation of NO, NO_2, and soot remains a key pollutant problem during liquid hydrocarbon combustion. It is well recognized that many important combustion phenomena such as ignition, pollutant formation, and efficiency are kinetically controlled, and, under the wide range of operating conditions encountered in gas turbine combustors (equivalence ratio, temperature, and pressure, for example), a knowledge of the intermediate combustion products is highly desirable. However, in comparison to simple fuels such as hydrogen, methane, or propane, very little effort has been made to predict the combustion of commercial fuels using detailed chemical kinetics. A complete combustion model should include a description of fluid mechanics coupled with detailed chemical kinetics of the combustion reactions. Thus, appropriately predictive computer models can be, when used judiciously, a most important design tool.

In the case of commercial fuels such as kerosene, this approach is computationally prohibitive because of the large number of species and reactions involved. The very complexity of a fuel like kerosene (comprising a mixture of *n*-alkanes, cycloalkanes, and aromatics) has necessarily restricted the modeling of its combustion in practical devices to the use of single-step empirical expressions or global multistep schemes to describe the chemistry. The main disadvantage of such models is that their validity is usually limited to a narrow parameter space of calibration. They are, however, often applicable to situations where mixing is the dominant process.

In recent years some experimental studies of kerosene combustion/oxidation have been reported, and a limited number of reaction mechanisms have been proposed.[1–6] These investigations have been concerned primarily with premixed systems, but turbulent diffusion flames are more commonly encountered in realistic combustion environments. The primary objective of this study is to compute the structure of strained counterflow kerosene diffusion flames. Understanding the structure and extinction of strained laminar flames is critical to the development and application of laminar flamelet concepts to turbulent flame propagation.[7] Considering the turbulent diffusion flame to be an ensemble of fluctuating laminar flamelets, the properties of which can be calculated separately, allows the incorporation of complex chemistry into the treatment of turbulent reacting flows.

Cathonnet and coworkers[1–3] have experimentally investigated the oxidation of both kerosene and *n*-decane in a jet-stirred reactor (JSR) under a wide range of conditions. Based on a strong similarity between the two fuels, they used a detailed chemical kinetic reaction mechanism describing the oxidation of *n*-decane to reproduce their experimental results for kerosene.[2,3] This was an advance on their previous study in which the kerosene oxidation was modeled using a quasi-global model.[1] Recently, the mechanism has been extended[8] by the addition of detailed submodels describing cyclohexane and toluene oxidation.

These investigations are complemented by the work of Vovelle et al.[4] and Douté et al.[5] who have compared the chemical structure of both *n*-decane and kerosene rich premixed flames stabilized on a flat-flame burner at atmospheric and reduced pressures. The

Received 20 November 1999; revision received 26 May 2000; accepted for publication 12 June 2000.

*Senior Research Fellow, Department of Fuel and Energy.
†Graduate Student, Department of Fuel and Energy.
‡Professor, Department of Fuel and Energy.
§Livesey Professor, Department of Fuel and Energy.
¶Technical Area Leader, Combustion and Environment Group, Propulsion Performance Department.

low-pressure kerosene flame was simulated[4] by assuming the initial fuel to be a mixture of *n*-decane and toluene, adding some reactions to describe benzene formation from toluene destruction to a detailed reaction mechanism for *n*-decane combustion. The *n*-decane component of the mechanism has recently been validated against the atmospheric pressure flame.[9] To the best of the present authors' knowledge, the kerosene oxidation mechanism developed to predict combustion in the premixed configuration has not been applied to the JSR geometry or vice versa.

Recently, Lindstedt and Maurice[6] have developed a detailed chemical kinetic reaction mechanism to account for the gas-phase chemistry of model practical aviation fuels. They have shown that the structure of kerosene flames can be predicted reasonably well using *n*-decane/alkyl substituted aromatic surrogate blends. They also demonstrated that the predictions for all major species using their model were independent of the nature of the initial aromatic species in the surrogate kerosene.

Unfortunately, the mechanisms are becoming more elaborate and increasingly complex, approaching up to 1100 elementary reactions involving some 200 distinct species. One-dimensional diffusion flame calculations even become computationally intense at these levels, to the extent of being unable to obtain stable converged solutions, particularly under increasing degrees of strain and pressure when using inlet conditions representative of realistic combustion environments. The results of numerical calculations of a strained kerosene-air diffusion flame employing a detailed reaction mechanism developed by the authors are reported in this paper. The effect of including a thermal radiation model on the flame structure under conditions of varying pressure and strain rate is also explored.

It is eminently useful to develop a model that will predict the combustion characteristics of kerosene under as wide a range of conditions as possible. Such a mechanism can be used in a network of interconnected reactor modules—combinations of plug flow, well-stirred, premixed, and nonpremixed jet reactors. To achieve this, a kinetic model of moderate size is necessary. This study presents a chemical reaction mechanism to simulate kerosene combustion under diffusion flame conditions that maintains enough detail to describe high-temperature experiments, including the major species profiles. The mechanism is also shown to predict satisfactorily species composition profiles in both spatially homogeneous and one-dimensional premixed combustion environments.

Computational Models

The modeling computations were performed using the CHEMKIN II suite of software[10] in conjunction with the PREMIX,[11] PSR,[12] and OPPDIF[13] programs. The governing equations for the preceding range of combustion regimes have already been well documented and will not be discussed in detail here; the reader is referred to the relevant reports for further information.

Premix

The laminar premixed flame structure calculations were performed using the PREMIX code for burner stabilized flames with a known mass-flow rate. The experimentally measured temperature profile was used in the calculations instead of solving the energy conservation equation. This eliminates the need to model heat losses to the burner, which may be significant. The chemistry is strongly temperature dependent, and the existence of an accurately measured temperature profile enables conclusions to be drawn about the chemical kinetic behavior. It also facilitates the comparison between calculated and measured species concentration profiles. Species concentrations as a function of distance from the burner surface are computed.

Perfectly Stirred Reactor

The perfectly stirred reactor (PSR) code was used to calculate the species concentrations for the JSR study. The well-stirred reactor is characterized by a reactor volume, residence time or a mass-flow rate, heat loss or a gas temperature, an inlet temperature, and mixture composition. The underlying assumption is that the mixing process is infinitely fast; the conversion of reactants to products is controlled solely by chemical reaction. As a consequence, no spatial temperature or concentration gradients are encountered.

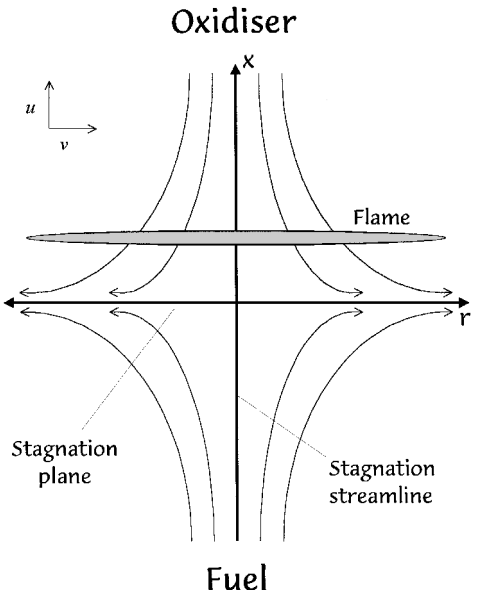

Fig. 1 Schematic illustration of a counterflow diffusion flame. The line drawn along the *r* axis represents the stagnation plane, and the dotted region suggests the flame.

OPPDIF

The OPPDIF code computes the structure of the diffusion flame stabilized in the vicinity of the stagnation plane formed between two impinging, laminar, axisymmetric, opposed streams. A schematic illustration of a counterflow flame is shown in Fig. 1. It consists of two infinitely wide circular nozzles directed toward each other at a fixed separation. When one stream contains fuel and the other air, a diffusion flame is stabilized on the oxidizer side of the stagnation plane as most fuels require more air than fuel by mass; the fuel diffuses through the stagnation plane to establish the flame in a stoichiometric mixture. OPPDIF solves for the temperature, species, mass fractions, axial and radial velocity components, and the radial pressure gradient.

The structure of the flame can be obtained as the solution of a set of coupled nonlinear two-point boundary-value problems along the stagnation streamline. In the counterflow configuration the temperature and composition profiles are one-dimensional and vary along the coordinate normal to the flame sheet. The freestream tangential and transverse velocities at the edge of the boundary layer are given by $v_\infty = ar$ and $u_\infty = -2ax$. The strain rate at the oxidizer inlet is generally used to characterize the flames. Jet velocities are input for both fuel and oxidizer such that the following condition is satisfied:

$$\left.\frac{\mathrm{d}u}{\mathrm{d}x}\right|_{\text{fuel}} = \sqrt{\frac{\rho_{\text{oxid}}}{\rho_{\text{fuel}}}}\left.\frac{\mathrm{d}u}{\mathrm{d}x}\right|_{\text{oxid}} \tag{1}$$

The computational mesh is determined adaptively. The energy equation was modified to take account of thermal radiation from water vapor and carbon dioxide. Using the optically thin approximation, a radiative heat loss term was estimated according to Hottel and Sarofim[14]:

$$Q = 4\sigma\kappa\left(T^4 - T_b^4\right) \tag{2}$$

Flame structures were computed both adiabatically and including the radiative transfer heat loss.

Reaction Mechanism

When formulating a reaction mechanism representative of kerosene combustion, a simplified model kerosene composition needs

to be identified. It is known that the composition of kerosene varies depending on quality and grade but, broadly speaking, can be considered to be made up of approximately 79% *n*-alkanes, 10% cycloalkanes, and 11% aromatics.[1,3] For the purposes of this study, the fuel is specified as a mixture of 89% *n*-decane and 11% toluene in order to simplify the mechanism and to rely on existing kinetic data. Klotz et al.[15] have already demonstrated that the chemical interactions between various components in a blend are limited to radical pool effects, and thus a mechanism for kerosene can then be formulated by combining individual schemes for *n*-decane and toluene. The authors, in this instance, have eschewed the construction of a reaction mechanism in a sequential, hierarchical manner. The *n*-decane part of the reaction scheme was developed using the approach outlined by Warnatz.[16] Here, the alkane is initially attacked by radicals or undergoes thermal decomposition. The alkyl radicals formed in the initial attack decompose via β-scission and fast thermal elimination of alkenes. This is considered to be the only relevant reaction of the higher alkyl radicals. Possible isomerization reactions are also neglected. The assumption employed here is that the alkyl radical decomposition and the reactions leading to C_1 and C_2 fragments are too fast to be rate limiting. The main purpose is to use the mechanism to explain phenomena such as NO_x formation or production of soot precursors for which a detailed C_1/C_2 chemistry is required.

A consideration of all possible isomers of *n*-decane and also those of product species is a daunting task, eased, however, by an examination of the experimental results. Guéret et al.[1] found that the main hydrocarbon intermediates formed during kerosene oxidation in a JSR were, in decreasing order of magnitude, ethene, propene, methane, 1-butene, 1,3-butadiene, ethane, and ethyne. Larger 1-olefins were among minor products and only found to accumulate during the early stages of the reaction. Douté et al.[5] also found that ethene was the most abundant olefin formed and by analysis of the relative ratios of the product olefins deduced that initial hydrogen abstraction was favored on the second or third carbon of the *n*-decane molecule. The relevant reactions may be summarized by the following sequence where two distinguishable *n*-decyl radicals are generated, following initial attack by radical species:

$$C_{10}H_{22} \xrightarrow{H,OH,O,HO_2,CH_3} 2-C_{10}H_{21} \rightarrow C_3H_6 + 1-C_7H_{15} \quad (3)$$

$$C_{10}H_{22} \xrightarrow{H,OH,O,HO_2,CH_3} 3-C_{10}H_{21} \rightarrow 1-C_4H_8 + 1-C_6H_{13} \quad (4)$$

The parent *n*-decane also decomposes thermally by scission of a carbon-carbon bond to generate *n*-alkyl radicals. Further β-scission of the alkyl radicals formed will then yield ethene and smaller alkyl radicals. In the absence of any experimentally measured kinetic rate data for thermal decomposition and hydrogen abstraction reactions of *n*-decane, the rate coefficients for these reactions were determined using the procedure of Axelsson et al.[17] A total of 14 reactions were used to break down the parent *n*-decane molecule into smaller alkyl radicals and olefins.

The chemistry of C_1, C_2, and C_3 hydrocarbons, being comparatively well understood, comprises the bulk of the mechanism being based on the GRI Mech 2.11 (see http://www.me.berkeley.edu/gri_mech) and also the heptane mechanism of Davis and Law.[18] The nitrogen chemistry of the GRI Mech 2.11, including thermal, prompt, and reburn mechanisms, was retained. The toluene oxidation mechanism, which also includes a benzene submodel, is taken from the study of Emdee et al.[19] using updated rate coefficients from Davis et al.[20] The final reaction mechanism consists of 440 mainly reversible reactions of 84 species. In this study all calculations were performed without any modification of the kinetic parameters.

Reverse-rate coefficients were calculated using thermodynamic properties mainly taken from the CHEMKIN database,[21] the compilation of Burcat and McBride,[22] and from Emdee et al.[19] Thermodynamic data for the larger alkanes and *n*-alkyl radicals were estimated using the group additivity methods of THERM.[23] The CHEMKIN transport database[24] was used, and, when not available, transport data were estimated using the methods outlined by Wang and Frenklach.[25]

The mechanism is initially validated using the experimental data of Dagaut et al.[3] and Douté et al.,[5] representing increasing degrees of complexity. The JSR data test the rigor of the model under high-pressure conditions, whereas the premix data introduce an extra dimension in the form of a spatial or temporal coordinate of the concentration of reactants, intermediates, and products. The scheme is then used to compute the structure of counterflow kerosene diffusion flames.

Numerical Modeling Results

In all of the cases discussed next, the same reaction mechanism that was outlined in the preceding section was used, without any modification, in moving from one combustion regime to the next. The only differences were based on the particular configuration of a system, whereas the chemistry involved remained the same and in all cases kerosene is represented by a mixture comprising 89% *n*-decane and 11% toluene.

JSR

The authors of Refs. 1–3 and 8 have used a JSR to study kerosene oxidation under a wide range of conditions. Highly diluted fuel (0.025 to 0.1% by volume) at equivalence ratios ranging from 0.5 to 1.5 was oxidized in a 35 cm^3 fused silica reactor at temperatures from 550 to 1200 K. Mean residence times varied from 0.5 to 2.0 s, and pressures up to 40 atm were employed. Because of the high dilution of reactants, operation at steady state is possible. Temperatures were measured using an uncoated chromel-alumel thermocouple of 0.16-mm diam without further correction. There was a negligible temperature rise as a result of reaction. A wide range of gas chromatographs equipped with various detectors was employed to analyze the oxidation products. The temperature range below 750 K was ignored for the purposes of this modeling study as it represents the area of negative temperature coefficient. It is also associated with the formation of several oxygenated products characteristic of the cool flame regime.

References 1–3 and 8 show that, under similar experimental conditions, both kerosene and *n*-decane fuels gave very similar concentration profiles for the main oxidation products. Interestingly, in one study[1] they also investigated the oxidation of a "model kerosene," a ternary mixture composed of *n*-undecane, *n*-propylcyclohexane, and trimethylbenzene, and found that the reactivity and reaction products formed were essentially identical to those of the original kerosene fuel. This representation of kerosene by an equivalent mixture of pure hydrocarbons representing the main families of chemical species certainly simplifies the modeling process of such a multicomponent fuel.

Two experimental conditions were chosen as input to the calculations. These were 1) $P = 10$ atm, $\phi = 1.5$, $\tau = 0.5$ s, and an initial fuel mole fraction of 10^{-3}; and 2) $P = 40$ atm, $\phi = 1.0$, $\tau = 2.0$ s, and an initial fuel mole fraction of 2.5×10^{-4}. Calculations were performed at various temperatures between 750 and 1200 K depending on the input conditions, and the results are presented in Fig. 2. The experimental results of Cathonnet et al.[8] under identical conditions are shown for comparison. The model predicts the concentration profiles as a function of temperature for the major species O_2, CO_2, and CO very well at both pressures, for rich and stoichiometric mixtures and for long and short residence times. The intermediate species H_2, CH_4, C_2H_4, C_3H_6, and 1-C_4H_8 are extremely well predicted as is the major oxygenated species, formaldehyde. There are some slight discrepancies in the comparison between computed and measured C_6H_6 and C_2H_2 profiles, and the largest deviation occurs between calculated and experimental C_2H_6 profiles. As the experimental data are presented without addressing the accuracy of the species analysis and measurement, the overall agreement between model and experiment can be considered quite remarkable.

The mechanism proves to be just as effective as that developed by Cathonnet et al.,[8] as evidenced by a comparison of the computed kerosene profiles from this study and from Ref. 8. In both

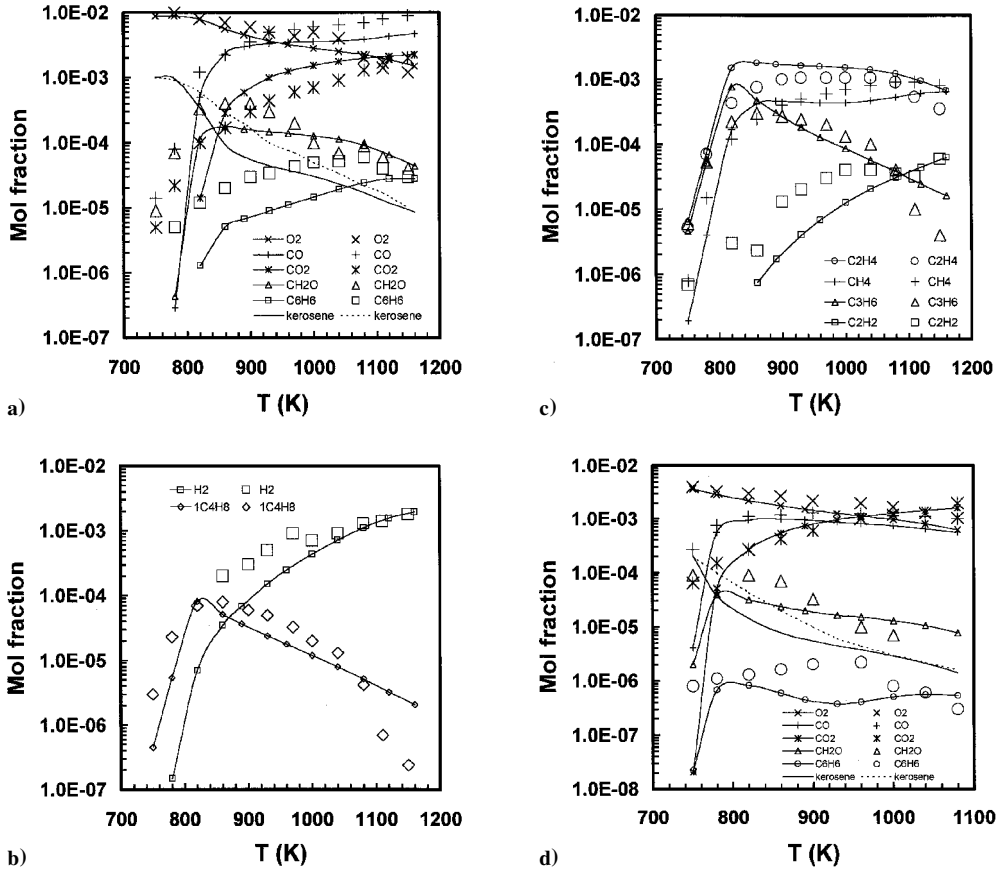

Fig. 2 Concentration profiles obtained for kerosene oxidation in a JSR under different conditions of pressure, equivalence ratio, and residence time: a) P = 10 atm, ϕ = 1.5, and τ = 0.5 s; b) P = 10 atm, ϕ = 1.5, and τ = 0.5 s; c) P = 10 atm, ϕ = 1.5, and τ = 0.5 s; and d) P = 40 atm, ϕ = 1.0, and τ = 2.0 s. The —— with small symbols represent the results of the calculations of this study, and the large symbols are the experimental data of Cathonnet et al.[8] The - - - - shown in a) and d) are the kerosene profiles from Ref. 8.

cases kerosene is represented by surrogate mixtures, here by 89% n-decane + 11% toluene and in Ref. 8 by 78% n-decane + 9.8% cyclohexane + 12.2% toluene. The kerosene decay profile calculated using the present model is only slightly faster than that presented in Ref. 8. This is quite instructive as the present reaction mechanism is much smaller and completely neglects the formation and subsequent reactions of 1-olefins with more than four carbon atoms.

Premixed Flames

Vovelle et al.[4] have determined the structure of rich premixed kerosene/O_2/Ar flames ($\phi = 2.2$) stabilized at low pressure (0.06 atm) on a flat flame burner. Mole fraction profiles of stable and radical species were measured using a molecular beam mass spectrometry technique and temperature was measured using a Pt-Pt 10% Rh thermocouple. The goal of that study was to identify the primary source of aromatic compounds and soot precursors in kerosene flames. Douté et al.[5] extended the investigation to the chemical structure of atmospheric rich premixed kerosene/O_2/N_2 flames ($\phi = 1.7$) using, in this case, gas chromatography for the identification of stable species. Temperature measurements were also made along the flame's symmetry axis using a Pt-Pt 10% Rh thermocouple. The flame was described as possessing a very faint luminosity caused by soot when observed in darkness. They found that the change in pressure from 0.06 to 1.0 atm did not change the main features of the chemical structure of the flame.

A close similarity was observed for the concentration profiles in the premixed flames of both kerosene and n-decane fuels at similar pressures; the only marked difference being that the amount of benzene formed in the kerosene flame exceeds that found in the n-decane flame by an order of magnitude. This obviously results from the presence of aromatic components in the kerosene fuel. In addition, the temperature of the kerosene flame was found to be higher by about 50 K. This emphasizes the necessity of including an aromatic component in the mechanism. The atmospheric pressure flame was chosen as a basis for comparison with the model as an experimental temperature profile is provided along with extensive mole fraction profiles of major and intermediate species.

The experimental temperature profile of Douté et al.[5] was introduced as input data in the calculations. The quoted accuracy of the temperature measurements is ±0.1 mm for position and ±5% for the temperature signal. The input premixed fuel/oxidizer mixture was 2.95% kerosene, 28.64% O_2, and 68.4% N_2, and a mass-flow rate of 0.0099 g cm^{-2} s^{-1} was employed. The calculated mole fraction profiles of a selection of major species as a function of distance from the burner surface are shown in Figs. 3–5. The measured data of Douté et al.[5] are also presented for comparison. Douté et al.[5] have discussed the difficulties encountered in the H_2O analysis and hence have given an estimation of the accuracy of the analysis as 6% for major species (O_2, N_2, CO, CO_2, H_2, H_2O) and as 12% for all other species (these are shown as error bars in Figs. 3–5). Taking this into consideration, the predictions of the model are quite satisfactory, although the C_2H_2 profile is slightly underpredicted and the C_2H_4 slightly overpredicted (Fig. 4). The possibility of a temperature sensitivity of the profiles was explored by increasing and decreasing the temperature by 5%, the quoted error. The results are shown for the C_6H_6 profiles in Fig. 5. Spatially, the profile shape seems to be better captured by the higher temperature, the benzene decay downstream exhibiting quite a sensitivity to temperature.

Counterflow Diffusion Flames

The computations were performed on a finite computational domain of 1.0 cm, that is, a jet separation of 1.0 cm. The fuel input was 100% kerosene (as already defined) at an initial temperature

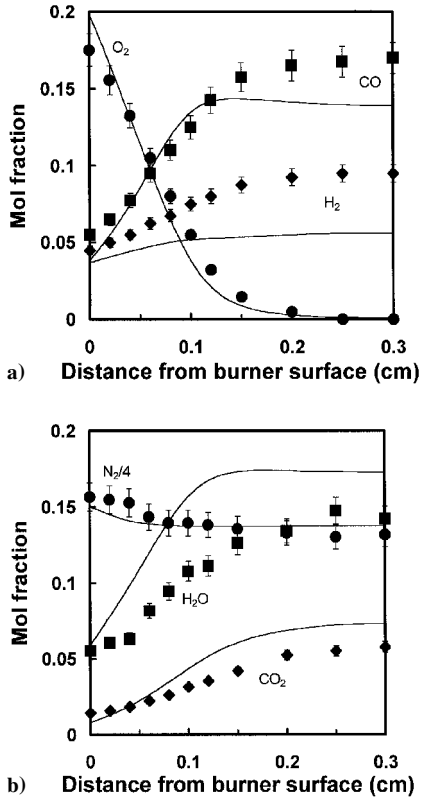

Fig. 3 Concentration profiles of a) O_2, CO and H_2 and b) N_2, H_2O and CO_2 as a function of distance from the burner surface for a rich atmospheric premixed kerosene flame. The —— represent the results of the calculations from this study, and the symbols are the measured experimental data, including error bars, of Douté et al.[5]

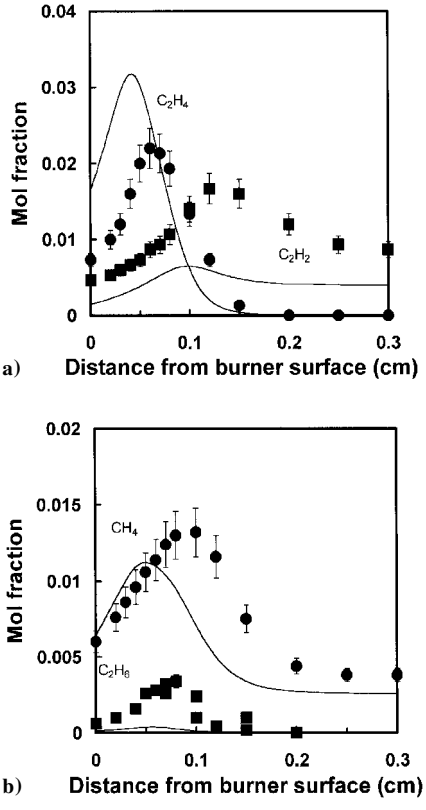

Fig. 4 Concentration profiles of a) C_2H_4 and C_2H_2 and b) CH_4 and C_2H_6 as a function of distance from the burner surface for a rich atmospheric premixed kerosene flame. The —— represent the results of the calculations from this study, and the symbols are the measured experimental data, including error bars, of Douté et al.[5]

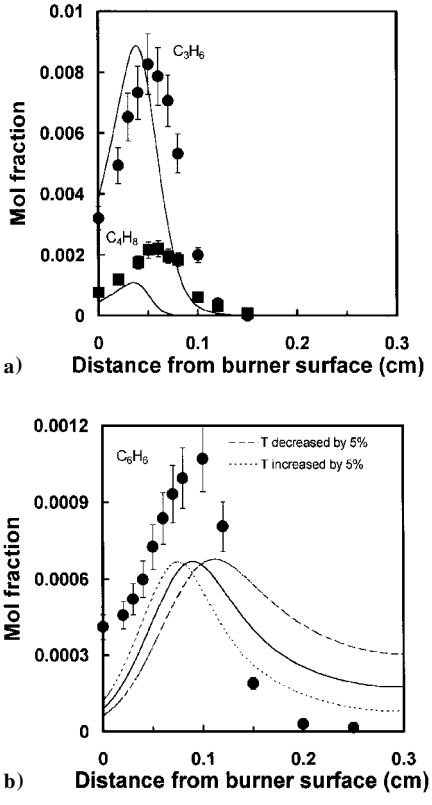

Fig. 5 Concentration profiles of a) C_3H_6 and C_4H_8 and b) C_6H_6 as a function of distance from the burner surface for a rich atmospheric premixed kerosene flame. The —— represent the results of the calculations from this study, and the symbols are the measured experimental data, including error bars, of Douté et al.[5] The - - - - and · · · · lines in b) illustrate the effect of changing the temperature by the quoted error margins of ± 5%.

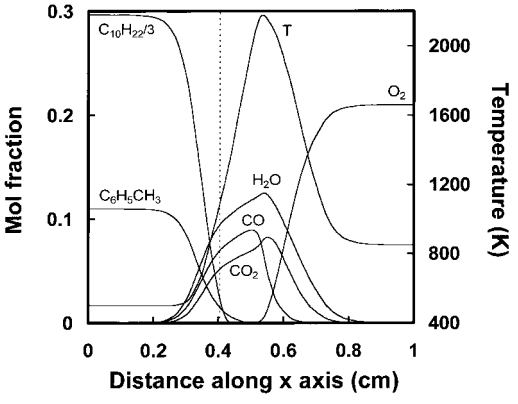

Fig. 6 Species and adiabatic temperature profiles along the stagnation streamline (x axis in Fig. 1), $a = 100\,s^{-1}$ and $P = 1$ atm. The vertical - - - - represents the location of the stagnation plane.

of 500 K to represent fully vaporized fuel. The oxidizer jet comprised air (21% O_2 + 79% N_2 by volume) at an initial temperature of 850 K. These temperatures are representative of an aircraft gas turbine combustor. The flame structure calculated for a weakly strained flame, $a = 100\,s^{-1}$, at atmospheric pressure is shown in Fig. 6, where mole fractions and adiabatic temperature are plotted against distance along the stagnation streamline. Here, $x = 0$ cm represents the fuel inlet, and $x = 1$ cm represents the air inlet. The vertical dashed line signifies the location of the stagnation plane. The flame has established itself on the air side, at a distance of approximately 0.12 cm from the stagnation plane.

Figure 6 actually shows the variation of the profiles along the x coordinate in physical space. The resulting flame is quite thin,

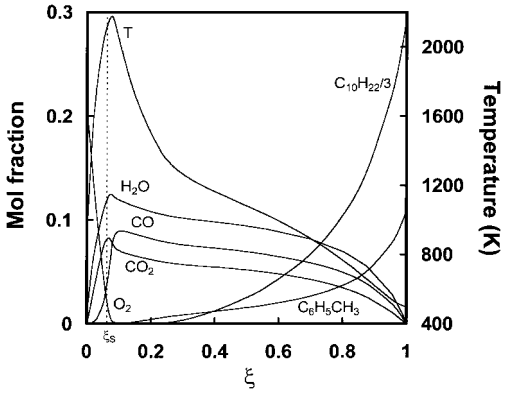

Fig. 7 Species and adiabatic temperature profiles as a function of mixture fraction, $a = 100\ s^{-1}$ and $P = 1$ atm. The vertical - - - - represents the stoichiometric mixture fraction.

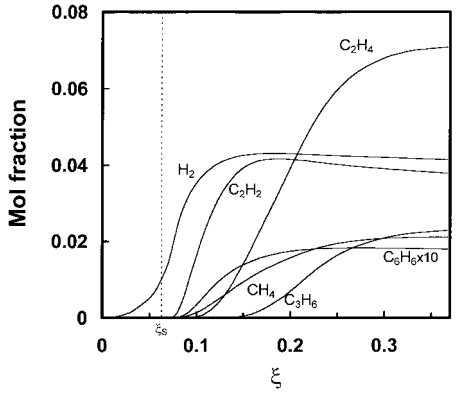

Fig. 8 Concentration profiles of major hydrocarbon intermediate species as a function of mixture fraction under adiabatic conditions, $a = 100\ s^{-1}$ and $P = 1$ atm. The vertical - - - - represents the stoichiometric mixture fraction.

and to obtain more detailed information on the diffusion flame it is more convenient to map the composition and temperature profiles in mixture fraction ξ space, also a requirement for construction of flamelet libraries. Mixture fractions were calculated using the method of Bilger et al.[26] The structure of the flame is plotted against mixture fraction in Figs. 7 and 8; ξ has the property that it is zero in the air stream and one in the fuel stream. The vertical dashed line in these plots represents the stoichiometric mixture fraction. The adiabatic temperature maximum is located just on the rich side of ξ_S. Figure 8 shows that the major hydrocarbon product is ethene, followed by ethyne, propene, and methane. These are produced by the thermal decomposition of the parent fuel and by methyl radical attack primarily. All of these species are seen to be consumed before the stoichiometric mixture fraction. Hydrogen can be observed to break through the stoichiometric position and past the point of maximum temperature. The radicals OH, H, and O are plotted in Fig. 9, and, as would be expected, OH and O peak on the lean side of ξ_S whereas H peaks on the rich side. The NO mole fraction profile is also presented in this figure, and a comparison with Fig. 7 shows that the NO reaches a maximum at the same location as the temperature.

Effect of Pressure

Calculations were carried out where the strain rate was held constant at a value of $100\ s^{-1}$, and the pressure varied from atmospheric to 40 atm again under adiabatic conditions. An increase in the pressure results in a decrease in the reaction zone thickness and a shift of the flame closer to the stagnation plane. Maximum temperature and peak radical mole fractions are plotted in Fig. 10 as a function of pressure. The peak radical concentrationsshow a steady decrease with increasing pressure as a result of greatly enhanced three body

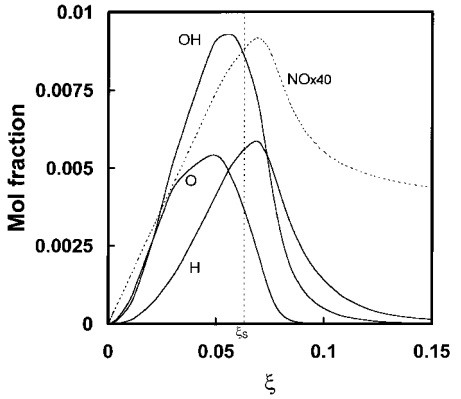

Fig. 9 Profiles of radical species and NO as a function of mixture fraction under adiabatic conditions, $a = 100\ s^{-1}$ and $P = 1$ atm. The vertical - - - - represents the stoichiometric mixture fraction.

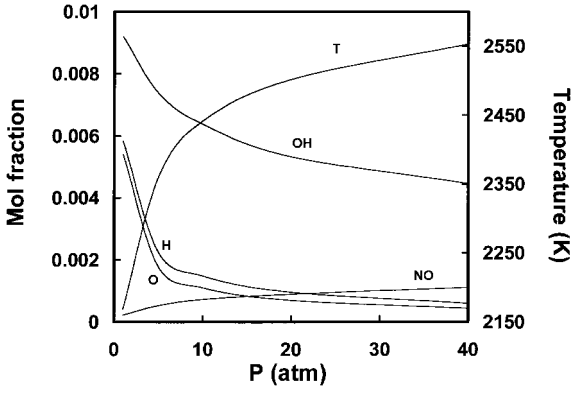

Fig. 10 Variation of peak mole fractions and maximum adiabatic temperature with pressure. The strain rate is maintained constant at $100\ s^{-1}$.

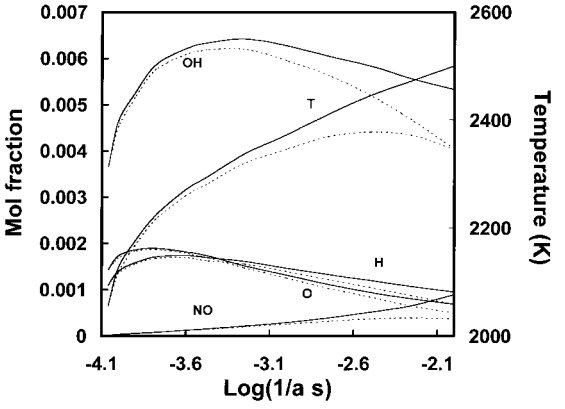

Fig. 11 Variation of peak mole fractions and maximum temperature as a function of reciprocal strain rate under adiabatic (——) and radiative heat loss (- - - -) conditions. The pressure is maintained constant at 20 atm.

recombination reactions. These reactions are highly exothermic, and so the temperature consequently exhibits an increase as the pressure is raised. The gradual rise in NO maximum concentration is also accompanied by a shift in the maximum from the rich side of stoichiometric at atmospheric pressure to the lean side at 40 atm, suggesting a change of mechanism as the pressure is increased.

Effect of Strain Rate

Calculations were also performed where the pressure was maintained constant at 20 atm and the strain rate progressively increased until extinction occurred. Figure 11 shows the maximum temperatures achieved at selected strain rates. As the strain rate is increased,

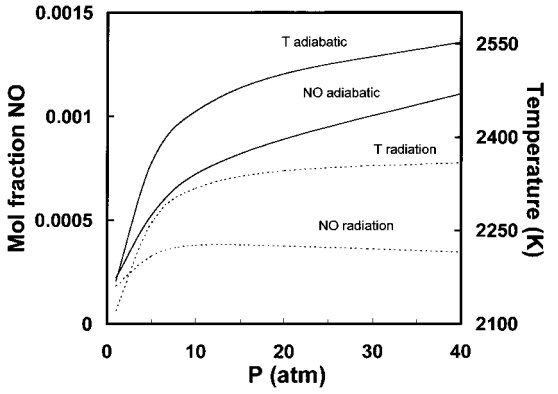

Fig. 12 Peak NO mole fractions and maximum temperature as a function of pressure computed under adiabatic (——) and radiative heat loss (- - - -) conditions. The strain rate is maintained constant at 100 s^{-1}.

the flame becomes thinner and moves closer to the stagnation plane. Flame structures, however, remained strikingly similar as the strain rate was increased. The temperature profiles within the flame also were alike although the peak temperature decreased with increasing velocity gradient. As the inlet velocities increase, the radial velocities increase correspondingly. This reduces the time available for the relatively slow recombination reactions to raise the temperature. The strain rate can thus be regarded as the inverse of a characteristic residence time in the reaction zone, and extinction occurs when there is insufficient time for reaction. Under the conditions of the calculation where the boundary temperatures of fuel and oxidizer were 500 and 850 K, respectively, extinction was found to occur at a strain rate of 11,500 s^{-1}. The extinction process was found to be quite abrupt with respect to flame structure: either there is a flame or there is not. It can also be seen in Fig. 11 that the peak mole fractions of the radical species pass through a maximum as the strain rate increases, whereas the NO simultaneously gradually decreases. As the flame progresses from the low strain structure, it is able to support higher reaction rates. The temperature effect on the reaction eventually overtakes the effect of increases in concentration of the reactants, which accounts for the appearance of the maxima in the peak radical profiles with respect to reciprocal strain rate. The lower temperatures in the reaction zones of the flames with higher strain rates are accompanied by a lower reactedness, that is, by an increased breakthrough of both fuel and oxygen past the positions of maximum temperature and the location of the stoichiometric mixture fraction.

Effect of Radiation

The energy equation was modified to take radiative heat losses from gas-phase species into consideration as this would be expected to assume greater importance at higher pressures because of increased concentrations of the radiating species. Selected results of these computations are given in Fig. 12, where they are compared with the corresponding calculations under adiabatic conditions using a strain rate of 100 s^{-1}. At atmospheric pressure thermal radiation has only a small influence on the predicted maximum temperature, and its effect on the concentration of major species is essentially negligible. Its effect, however, becomes quite pronounced as the pressure is increased. For example, the peak temperature drops approximately 200 K with a corresponding decrease by a factor of three for the peak NO concentration, as can be seen in Fig. 12. The influence of thermal radiation, as the strain rate is increased, on species concentrations and maximum temperature is shown in Fig. 11. The greatest loss caused by thermal radiation is observed to occur at the lowest strain rates; its effect being almost negligible at the higher strain rates.

Discussion

The present modeling study has shown that the combustion of kerosene can be quite adequately represented by a reaction mechanism developed assuming a surrogate kerosene fuel, composed of a mixture of pure hydrocarbons representative of its major components. The mechanism has been used to predict the combustion and oxidation of kerosene under PSR and premixed flame conditions. To the best of the authors' knowledge, this represents the first application of a detailed kinetic mechanism for a commercial fuel that has been validated against experimental results from more than one combustion regime. The agreement between computed and measured profiles is quite good in both cases, although the C_2 species predictions could be improved for both combustion environments. Although, in a few cases, there are significant discrepancies between the predicted and experimental values particularly in the modeling of the JSR at the lower temperatures, these are countered by the overall good qualitative reproduction of the experimental profiles and trends in the two combustion regimes. The kinetic parameters of the reaction mechanism were not optimized to improve the comparison between the predicted and experimental results. Clearly, the effect of the branching ratios in the initial decomposition steps of the parent *n*-decane and toluene fuel components will have a strong influence on the distribution of the lower hydrocarbons encountered in the burnt gases. A detailed sensitivity analysis and reaction pathway breakdown is required to reproduce better the experimental data. Additionally, a lot more experimental data under a wide variety of conditions would be most instrumental in trying to pin down the combustion kinetics of commercial fuels. The satisfactory agreement obtained between the experimental and computed JSR data extends the domain of validity of the mechanism to high-pressure conditions.

This mechanism was also used, with no further modification, to predict the structure of a kerosene/air counterflow diffusion flame, although the authors do recognize the fact that it has been noted that the GRI Mech 2.11 may do a rather poor job of reproducing C_2 hydrocarbon species in counterflow and coflow systems. The temperature profile in this case is determined by solving the energy equation, unlike for the PSR and PREMIX configurations, where experimentally measured temperatures were available and input as an initial condition. Radiation losses, therefore, need to be included. The results presented in this study show how important the gas-phase radiative losses become as the pressure is increased. Thermal radiation reduces the local temperature sufficiently to affect the production rate of NO, as was clearly evident in Fig. 12. Incorporation of the thermal radiative heat loss into the laminar flamelet can simplify the treatment of turbulence-chemistry models for practical diffusion flames.

Conclusions

A chemical kinetic reaction mechanism, which uses a mixture of 89% *n*-decane and 11% toluene to represent the kerosene chemically, was developed for kerosene combustion. The mechanism was initially tested against experimental premixed flame data and jet-stirred reactor data. The comparison between the experimental data and the calculated concentration profiles was found to be quite good. The mechanism was used to predict the structure of a counterflow kerosene/air diffusion flame under conditions of varying pressure and strain rate. As the pressure is increased, the temperature increases significantly with a subsequent decrease in peak concentrations of radical species. When keeping the pressure constant and increasing the strain rate of the flame, the peak temperature decreases until the point of extinction is reached. The inclusion of a radiative heat loss model incorporating thermal radiation from CO_2 and H_2O was found to have a profound effect on the calculated temperature and predicted NO levels, particularly under conditions of high pressure and low strain.

Acknowledgments

The authors would like to thank Package 7b of the UK MOD and the UK DTI for funding and permission to publish this work. The authors also acknowledge the assistance of Y. B. Yang with the implementation of the radiation model.

References

[1]Guéret, C., Cathonnet, M., Boettner, J. C., and Gaillard, F., "Experimental Study and Modelling of Kerosene Oxidation in a Jet-Stirred Flow

Reactor," *Proceedings of the Twenty-Third International Symposium on Combustion*, Combustion Inst., Pittsburgh, PA, 1990, pp. 211–216.

[2]Dagaut, P., Reuillon, M., Boettner, J. C., and Cathonnet, M., "Kerosene Combustion at Pressures up to 40 Atm: Experimental Study and Detailed Chemical Kinetic Modelling," *Proceedings of the Twenty-Fifth International Symposium on Combustion*, Combustion Inst., Pittsburgh, PA, 1994, pp. 919–926.

[3]Dagaut, P., Reuillon, M., Cathonnet, M., and Voisin, D., "High Pressure Oxidation of Normal Decane and Kerosene in Dilute Conditions from Low to High Temperature," *Journal de Chimie Physique*, Vol. 92, No. 1, 1995, pp. 47–76.

[4]Vovelle, C., Delfau, J. L., and Reuillon, M., "Formation of Aromatic Hydrocarbons in Decane and Kerosene Flames at Reduced Pressures," *Soot Formation in Combustion: Mechanisms and Models*, edited by H. Bockhorn, Springer-Verlag, Berlin, 1994, pp. 50–65.

[5]Douté, C., Delfau, J. L., Akrich, R., and Vovelle, C., "Chemical Structure of Atmospheric Pressure Premixed *n*-Decane and Kerosene Flames," *Combustion Science and Technology*, Vol. 106, Nos. 4–6, 1995, pp. 327–344.

[6]Lindstedt, P., and Maurice, L. Q., "A Detailed Chemical Kinetic Model for Aviation Fuels," *Journal of Propulsion and Power*, Vol. 16, No. 2, 2000, pp. 187–195.

[7]*Turbulent Reacting Flows*, edited by F. A. Williams and P. A. Libby, Academic, London, 1994.

[8]Cathonnet, M., Voisin, D., Etsouli, A., Sferdean, C., Reuillon, M., Boettner, J. C., and Dagaut, P., "Kerosene Combustion Modelling Using Detailed and Reduced Chemical Kinetic Mechanisms," *Proceedings of AGARD Conference*, 1998 (**to be published**).

[9]Douté, C., Delfau, J. L., and Vovelle, C., "Modelling of the Structure of a Premixed *n*-Decane Flame," *Combustion Science and Technology*, Vol. 130, Nos. 1–6, 1997, pp. 269–313.

[10]Kee, R. J., Rupley, F. M., and Miller, J. A., "CHEMKIN II: A Fortran Chemical Kinetics Package for the Analysis of Gas Phase Chemical Kinetics," Sandia National Lab., Sandia Rept. SAND89-8009, March 1989.

[11]Kee, R. J., Grcar, J. F., Smooke, M. D., and Miller, J. A., "A Fortran Program for Modelling Steady One-Dimensional Premixed Flames," Sandia National Lab., Sandia Rept. SAND85-8240, Dec. 1985.

[12]Glarborg, P., Kee, R. J., Grcar, J. F., and Miller, J. A., "PSR: A Fortran Program for Modelling Well-Stirred Reactors," Sandia National Lab., Sandia Rept. SAND86-8209, Feb. 1986.

[13]Lutz, A. E., Kee, R. J., Grcar, J. F., and Rupley, F. M., "OPPDIF: A Fortran Program for Computing Opposed-Flow Diffusion Flames," Sandia National Lab., Sandia Rept. SAND96-8243, May 1997.

[14]Hottel, H. C., and Sarofim, A. F., *Radiative Transfer*, McGraw–Hill, New York, 1967, pp. 199, 262.

[15]Klotz, S. D., Brezinsky, K., and Glassman, I., "Modelling the Combustion of Toluene-Butane Blends," *Proceedings of the Twenty-Seventh International Symposium on Combustion*, Combustion Inst., Pittsburgh, PA, 1998, pp. 337–344.

[16]Warnatz, J., "Chemistry of High Temperature Combustion of Alkanes up to Octane," *Proceedings of the Twentieth International Symposium on Combustion*, Combustion Inst., Pittsburgh, PA, 1984, pp. 845–856.

[17]Axelsson, E. I., Brezinsky, K., Dryer, F. L., Pitz, W. J., and Westbrook, C. K., "Chemical Kinetic Modelling of the Oxidation of Large Alkane Fuels: *n*-Octane and iso-Octane," *Proceedings of the Twenty-First International Symposium on Combustion*, Combustion Inst., Pittsburgh, PA, 1986, pp. 783–793.

[18]Davis, S. G., and Law, C. K., "Laminar Flame Speeds and Oxidation Kinetics of iso-Octane/Air and *n*-Heptane/Air Flames," *Proceedings of the Twenty-Seventh International Symposium on Combustion*, Combustion Inst., Pittsburgh, PA, 1998, pp. 521–527.

[19]Emdee, J. L., Brezinsky, K., and Glassman, I., "A Kinetic-Model for the Oxidation of Toluene Near 1200K," *Journal of Physical Chemistry*, Vol. 96, No. 5, 1992, pp. 2151–2161.

[20]Davis, S. G., Wang, H., Brezinsky, K., and Law, C. K., "Laminar Flame Speeds and Oxidation Kinetics of Benzene-Air and Toluene-Air Flames," *Proceedings of the Twenty-Sixth International Symposium on Combustion*, Combustion Inst., Pittsburgh, PA, 1996, pp. 1025–1033.

[21]Kee, J. F., Rupley, F. M., and Miller, J. A., "The Chemkin Thermodynamic Database," Sandia National Lab., Sandia Rept. SAND87-8215B, 1987.

[22]Burcat, A., and McBride, B., "Ideal Gas Thermodynamic Data for Combustion and Air Pollution Use," Technion, Rept. TAE804, Haifa, Israel, Dec. 1998.

[23]Ritter, E. R., "THERM: A Computer Code for Estimating Thermodynamic Properties for Species Important to Combustion and Reaction Modelling," *Journal of Chemical Information and Computer Science*, Vol. 31, No. 3, 1991, pp. 400–408.

[24]Kee, R. J., Dixon-Lewis, G., Warnatz, J., Cotrin, M. E., and Miller, J. A., "The Chemkin Transport Database," Sandia National Lab., Sandia Rept. SAND86-8246, Dec. 1986.

[25]Wang, H., and Frenklach, M., "Transport Properties of Polycyclic Aromatic Hydrocarbons for Flame Modelling," *Combustion and Flame*, Vol. 96, Nos. 1–2, 1994, pp. 163–170.

[26]Bilger, R. W., Stårner, S. H., and Kee, R. J., "On Reduced Mechanisms for Methane-Air Combustion in Nonpremixed Flames," *Combustion and Flame*, Vol. 80, No. 2, 1990, pp. 135–149.